JOURNAL OF GEOPHYSICAL RESEARCH, VOL. 115, A00F04, doi:10.1029/2009JA014610, 2010



# Amplitude and phase of nonlinear magnetospheric wave growth excited by the HAARP HF heater

M. Gołkowski,[1] U. S. Inan,[1] M. B. Cohen,[1] and A. R. Gibby[2]

Received 26 June 2009; revised 14 September 2009; accepted 22 September 2009; published 13 February 2010.

[1] The High Frequency Active Auroral Research Program (HAARP) HF ionospheric heater is used to inject ELF/VLF signals into the magnetosphere to study wave-particle interactions that lead to nonlinear amplification. HAARP-generated whistler mode "echoes" are observed after twice crossing the equatorial plane in magnetospheric ducts. The magnetospheric paths traversed by the signals are determined to be in the range $5.06 < L < 5.19$ with associated cold plasma densities of $177\ \mathrm{cm}^{-3} < N_{eq} < 185\ \mathrm{cm}^{-3}$. The amplitude and phase of the echoes are observed to exhibit exponential temporal increase. A decrease in input amplitude by 14 dB is observed to yield a delay in onset of nonlinear growth by ~1 s. Nonlinear theory of cyclotron resonant currents formed by electrons phase trapped in the potential well of the input wave is used to analyze the simultaneous evolution of amplitude and phase of the observations. The average nonlinear resonant current vector is found to rotate in relation to the input wavefields during growth, and the magnetospheric linear growth rate is estimated to be 31–45 dB/s.

**Citation:** Gołkowski, M., U. S. Inan, M. B. Cohen, and A. R. Gibby (2010), Amplitude and phase of nonlinear magnetospheric wave growth excited by the HAARP HF heater, *J. Geophys. Res.*, *115*, A00F04, doi:10.1029/2009JA014610.

## 1. Introduction

[2] Nonlinear amplification of whistler mode waves in the Earth's magnetosphere is well documented to occur both naturally and in response to signals of anthropogenic origin. Naturally occurring whistler mode chorus is one of the most intense electromagnetic waves in the magnetosphere and has been the subject of numerous studies since the first observations by *Storey* [1953]. At the same time, experiments involving the injection of extremely low frequency and very low frequency (ELF/VLF) waves from the Earth have demonstrated that the magnetosphere acts as a nonlinear amplification channel and can be probed in a controlled manner [*Helliwell*, 1988; *Gołkowski et al.*, 2008]. A comprehensive understanding of whistler mode wave amplification is necessary for shedding light on a wide range of issues in magnetospheric physics. For example, wave growth plays a central role in the energy exchange in the magnetosphere as manifested in the generation of hiss and chorus waves and acceleration of energetic particles [*Hayakawa and Sazhin*, 1992; *Sazhin and Hayakawa*, 1992; *Omura et al.*, 2007; *Omura and Summers*, 2006]. Likewise magnetospheric amplification is relevant in the context of controlled precipitation of radiation belt electrons since wave amplitude is a key parameter in pitch angle scattering [*Inan et al.*, 2003].

[3] Magnetospheric amplification of both natural and man-made radiation is driven by cyclotron resonant wave-particle interactions between whistler mode waves and counterstreaming energetic electrons. If the wave-particle interaction does not induce significant change in the energetic electron distribution, a linear treatment is appropriate and growth can be estimated directly from the anisotropy of the energetic electron distribution function [*Kennel and Petschek*, 1966]. However, whistler mode amplification is often characterized by nonlinear effects such as modification of the electron distribution and generation of wave frequencies different from that of the input wave. Numerical models and theoretical formulations of the nonlinear problem stress the importance of the inhomogeneity of the geomagnetic field and trapping of energetic electrons in the potential well of the input wave [*Nunn*, 1974; *Karpman et al.*, 1975; *Bell and Inan*, 1981; *Omura et al.*, 1991; *Trakhtengerts et al.*, 2003; *Hobara et al.*, 2000; *Omura and Summers*, 2006; *Omura et al.*, 2008; *Gibby et al.*, 2008].

[4] In studies involving man-made signals, observations of nonlinear amplification have been variously termed as artificially stimulated emissions [*Stiles and Helliwell*, 1975], the coherent wave instability [*Helliwell*, 1988], or most frequently, VLF triggered emissions [*Omura et al.*, 1991]. The terminology is unfortunate not only because of its diversity but also because it enforces a categorization between a triggering (or stimulating) signal and a signal being triggered (or stimulated). Some authors have found this distinction useful in explaining physical models and notably *Dowden et al.* [1978] seek to emphasize it by introducing the additional term of an "embryo emission" (EE). However, it can be argued that for a highly nonlinear feedback

[1]STAR Laboratory, Stanford University, Stanford, California, USA.
[2]Arion Systems Inc., Chantilly, Virginia, USA.


0148-0227/10/2009JA014610$09.00

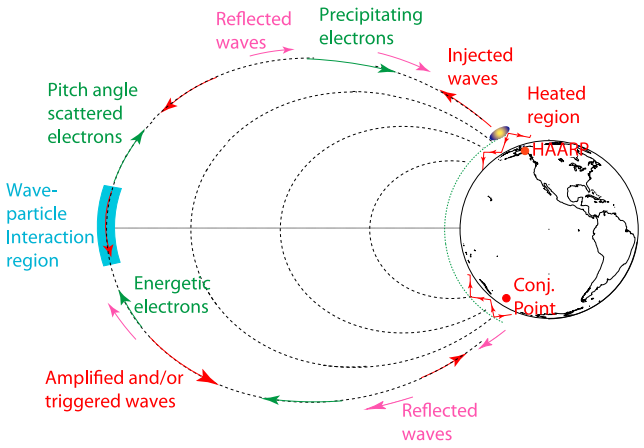


**Figure 1.** A schematic of the HAARP whistler mode wave injection experiment. ELF/VLF waves generated in the ionosphere above HAARP are injected into the Earth-ionosphere waveguide and into the magnetosphere.

process a rigid distinction between a driving wave and its amplified components is heuristic at best. Furthermore, it is hard to find consistency in the specific use of these terms in the literature. In most works on computer simulations authors identify a (triggered) emission upon the formation of radiating hot electron currents, but experimenters such as *Paschal and Helliwell* [1984] distinguish between temporal growth and associated "emissions" which are identified to commence upon rapid and sustained departure from the input frequency. To avoid confusion we have opted to use the more rigorously defined terms of linear and nonlinear magnetospheric amplification. The use of more fundamental terms does not obscure the physical processes and also facilitates the joint discussion of amplified waves with or without an apparent triggering source, which are commonly treated using the same theoretical formulations [*Omura et al.*, 2008; *Omura and Summers*, 2006].

[5] Despite the engineering challenge of generating ELF/VLF waves, controlled wave injection experiments have been pursued for several decades with the most referenced work performed by Stanford University at Siple Station, Antarctica ($L$~4.2) in 1973–1988. In its final state, the Siple Station experiment utilized a 42 km antenna driven by a ~1500 kW transmitter on a ~2 km thick ice sheet. ELF/VLF waves in the (~2–8 kHz) frequency range were injected into the magnetosphere with a rich collection of observations of ducted and nonlinearly amplified waves made in both northern and southern hemispheres before the closing of the station in 1988 [*Helliwell and Katsufrakis*, 1974; *Helliwell*, 1988; *Gibby*, 2008, and references therein]. More recently, controlled magnetospheric wave injection experiments have been conducted using the High Frequency Active Auroral Research Program (HAARP) heating facility in Gakona, Alaska (~62.4°N and 145.2°W geographic at $L$~5)[*Inan et al.*, 2003; *Gołkowski et al.*, 2008]. Unlike the conventional radio transmitter at Siple Station, generation of ELF/VLF signals with the HAARP facility is accomplished indirectly by modulating auroral electrojet currents in the ionosphere using HF (2–10 MHz) waves. The ELF/VLF radiation is believed to primarily result from modification of the ionospheric Hall conductivity and the radiation pattern is similar to that of a short dipole at 75–85 km altitude in the ionospheric D region [*Cohen et al.*, 2008]. The advantage of the HAARP experiment over analysis of legacy Siple Station data is that the HAARP facility is active and currently available for testing theory with new transmissions. Furthermore, the Siple Station transmitter required tuning to a relatively narrow frequency band [*Raghuram et al.*, 1974]. In contrast, the HAARP transmitter is not band limited facilitating experiments with large frequency ranges. Figure 1 shows the setup for the HAARP wave injection experiment. HAARP ELF/VLF waves are injected into the Earth-ionosphere waveguide and also into the magnetosphere. Field-aligned cold plasma density irregularities (magnetospheric ducts) guide the HAARP ELF/VLF signals to the magnetic equator. Amplified waves can be observed at the conjugate point where they are termed "1-hop echoes" or in the northern hemisphere after reflection from the conjugate ionospheric boundary where they are termed "2-hop echoes." Previous results show that the HAARP facility is most effective in injecting signals directly overhead [*Piddyachiy et al.*, 2008] and observations of amplification are most frequent when the plasmasphere extends to HAARP latitudes or higher [*Gołkowski et al.*, 2008]. Observation of magnetospheric amplification has been found to be sensitive to both the frequency band and the frequency-time format of the transmitted signal.

[6] We present new results from the HAARP wave injection experiment and focus on the evolution of amplitude and phase of the nonlinearly amplified signals to infer the dynamics of the nonlinear resonant currents in the interaction region. From observations of nonlinear amplification for two different input amplitudes, we propose a simple model to explain the differences in the observations. From this model, an experimental estimate of linear growth in the magnetosphere, which is a function of the anisotropy and flux of the resonant hot plasma distribution, is obtained.

## 2. Observations

[7] The observations described in this report were recorded with an AWESOME ELF/VLF receiver [*Cohen et al.*, 2009] located at Chistochina (62.61°N, 144.62°W), 37 km to the northeast of the HF facility. On 23 August 2007, the HAARP 3.25 MHz HF $X$ mode vertical beam was square wave amplitude modulated with 3 s long constant frequency tones and 500 Hz/s frequency-time ramps in the ELF band. During the times 2305–2332 UT, the HAARP generated signals were observed to return to the northern hemisphere as 2-hop echoes after propagating in field-aligned ducts and experiencing nonlinear magnetospheric amplification. Figure 2 shows two spectrograms from the magnetic field antenna oriented in the north-south direction at Chistochina, in which 2-hop echoes excited by HAARP ELF pulses and frequency-time ramps are evident. In Figure 2 (top) the transmission format is composed of 3 s pulses at 1110 Hz, 1590 Hz, and 930 Hz and a 500 Hz/s frequency-time ramp. The transmitted signals, along with their associated harmonics, are clearly seen as received at Chistochina. The 2-hop echoes are observed to be excited by the frequency-time ramp and the second harmonic of the 1110 Hz pulse at 2220 Hz. The 2-hop echoes are delayed ~7 s from their "parent" transmissions corresponding to two

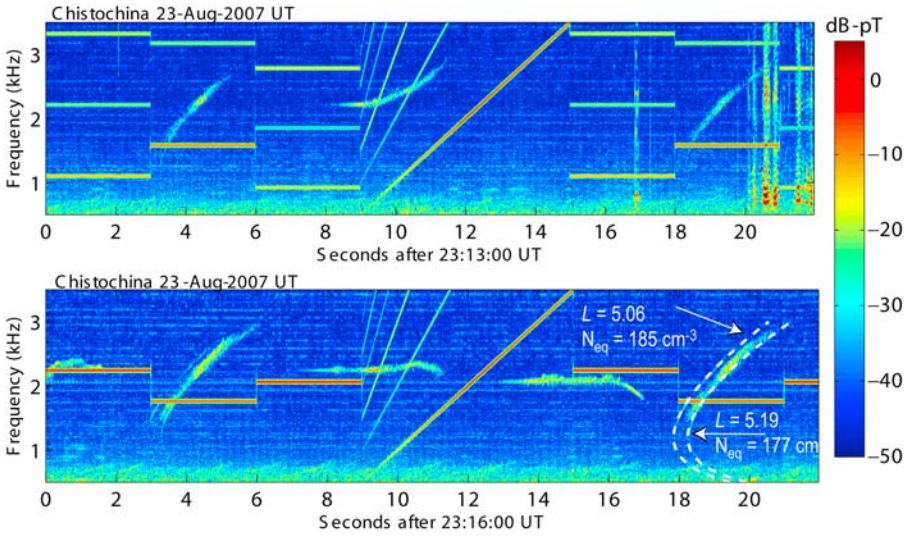


**Figure 2.** Spectrograms showing transmitted HAARP ELF signals and 2-hop echoes. Estimation of propagation path parameters from dispersion of frequency-time ramp echo shown on the bottom.

traversals of the equatorial plane in field aligned (or near field aligned) whistler mode propagation. Figure 2 (bottom) is from 3 min later after the frequencies of the tones in the transmission format were changed to 2250 Hz, 1770 Hz, and 2070 Hz to take advantage of the observed favorable magnetospheric response just above ~2 kHz. The frequency-time ramp is the same for both formats. In Figure 2 (bottom) 2-hop echoes are seen to be excited by the 2250 Hz and 2070 Hz pulses. Note that the 2250 Hz and 2070 Hz pulses in Figure 2 (bottom) are significantly higher in amplitude than the 2220 Hz second harmonic pulse in Figure 2 (top). For ELF signals generated by modulated HF heating, higher-order harmonics are known to be substantially weaker than fundamental tones [*Barr and Stubbe*, 1993]. The total horizontal magnetic field from the 2220 Hz second harmonic is found to be 13.8 dB weaker than the 2250 Hz fundamental tone transmitted 2 min later. The 2-hop echo excited by the weaker harmonic (2220 Hz) pulse is seen to arrive with an additional time delay relative to the 2-hop echoes triggered by the 2070 Hz and 2250 Hz pulses. No additional 2-hop echo delay is observed for the frequency-time ramps across both records. Variation in propagation delay for ducted signals is typically attributed to multiple propagation paths and variation in which path is dominant or most "active" [*Carpenter*, 1980]. Although the 2-hop echoes observed do exhibit multipath propagation, none of the determined paths yield sufficient delay characteristics to match the observation. The additional 2-hop echo delay for the weaker pulse is thus interpreted to result directly from the lower input amplitude as is discussed in section 3.

[8] The observation of 2-hop echoes excited by the frequency-time ramps allows for determination of the magnetospheric path and associated cold plasma density for these signals using whistler dispersion techniques [*Sazhin et al.*, 1992, and references therein]. The 2-hop echoes from the frequency-time ramps are observed to propagate along multiple magnetospheric paths. The dotted white lines in Figure 2 (bottom) are calculated dispersion curves assuming ducted parallel propagation with a dipole model of the geomagnetic field and the diffusive equilibrium model (DE-1) of cold plasma density [*Angerami and Thomas*, 1964]. The two curves bound the $L$ shells of the propagation paths and associated cold plasma densities traversed by the 2-hop echoes to $5.06 < L < 5.19$ and $177\ \mathrm{cm}^{-3} < N_{eq} < 185\ \mathrm{cm}^{-3}$. The 2-hop echoes triggered by the 2070 Hz and 2250 Hz pulses exhibit propagation delays consistent with the higher $L$ shell path. The magnetospheric paths are found to correspond to injection (or magnetospheric entry) locations very close to the heating facility consistent with previous results of HAARP induced VLF emissions [*Inan et al.*, 2003; *Gołkowski et al.*, 2008].

[9] Figures 3 and 4 present the variation of amplitude and phase of the 2-hop echoes triggered by the 2220 Hz harmonic and the 2250 Hz fundamental pulses. Figures 3a–3b and 4a–4b are spectrograms while Figures 3c–3d and 4c–4d show amplitude and Figures 3e–3f and 4e–4f show the phase offset from the phase reference at the transmitted frequency. The white dashed lines in Figures 3a–3b and 4a–4b and corresponding black lines in Figures 3c–3f and 4c–4f are reference lines showing constant delay from the time of transmission. The two red dashed lines respectively mark the onset of the observed 2-hop echoes and the end of the coherent growth phase of those echoes before the commencement of so-called frequency "risers" characterized by $df/dt > 0$. The amplitudes of both 2-hop echoes in Figure 3 are observed to increase at a rate of ~20 dB/s and saturate at an amplitude of 0.2 pT despite the 13.8 dB difference in input amplitude noted above. During the period of growth, the phase of the 2-hop echoes is seen to advance at a rate of 1–2 Hz. The cases shown in Figure 4 show very similar results. The key feature worth emphasizing is the simultaneous amplitude growth and phase advance. Such joint amplitude growth and phase advance observed here have been previously reported as characteristic of nonlinear magnetospheric amplification by *Paschal and Helliwell* [1984] and also by *Dowden et al.* [1978]. In fact,

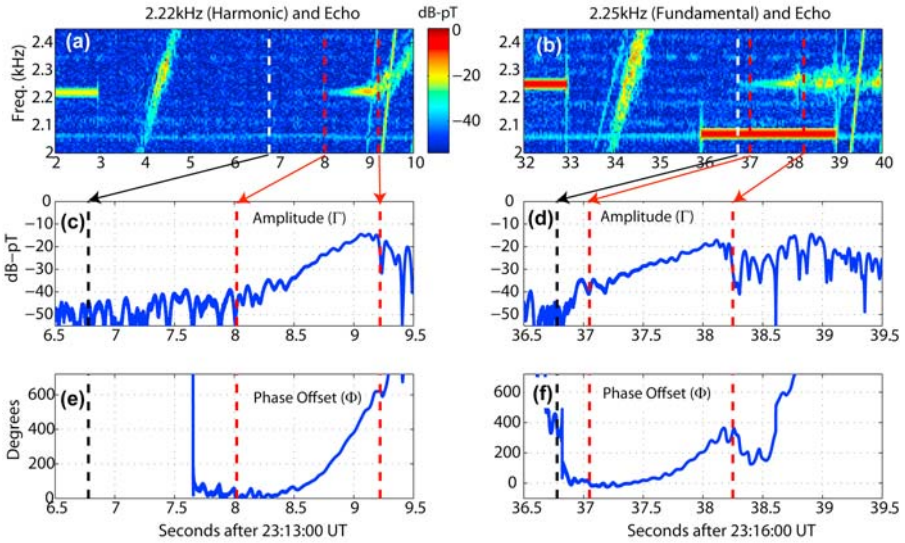


**Figure 3.** Observed amplitude and phase of 2-hop echoes resulting from transmissions of a (a, c, and e) second harmonic and (b, d, and f) fundamental tone. White dotted lines in Figures 3a and 3b correspond to black dotted lines in Figures 3c–3f, respectively.

*Paschal and Helliwell* [1984] report observations of nonlinear amplification, as well as rarer cases of "nongrowing" signals injected by the Siple transmitter. These rarer cases are distinguished by negligible phase advance and roughly constant amplitude observed at a ground based receiver. Similar distinctions between temporal and "nontemporal" amplification in the Siple experiment are noted by *Carpenter et al.* [1997]. In the HAARP wave injection experiment all 1-hop and 2-hop echoes observed thus far exhibit nonlinear amplification characterized by temporal amplitude growth and phase advance. The lack of observations of echoes exhibiting only linear amplification in the HAARP experiment is likely due to the lower amplitudes of ELF/VLF generated waves as compared to the Siple Station experiment, causing the signals without nonlinear amplification to remain below the noise floor.

## 3. Analysis and Interpretation

[10] The observations of *Paschal and Helliwell* [1984] from the Siple Station experiment highlight one of the principal difficulties in observing magnetospheric phenomena using ground based receivers. In particular, ground based receivers observe waves that have exited the magnetospheric interaction region. That is, any signal observed on the ground represents a wave that has interacted with the magnetospheric plasma over a range of time and space. For the case of a monochromatic input wave examined by *Paschal and Helliwell* [1984], constant growth predicted by

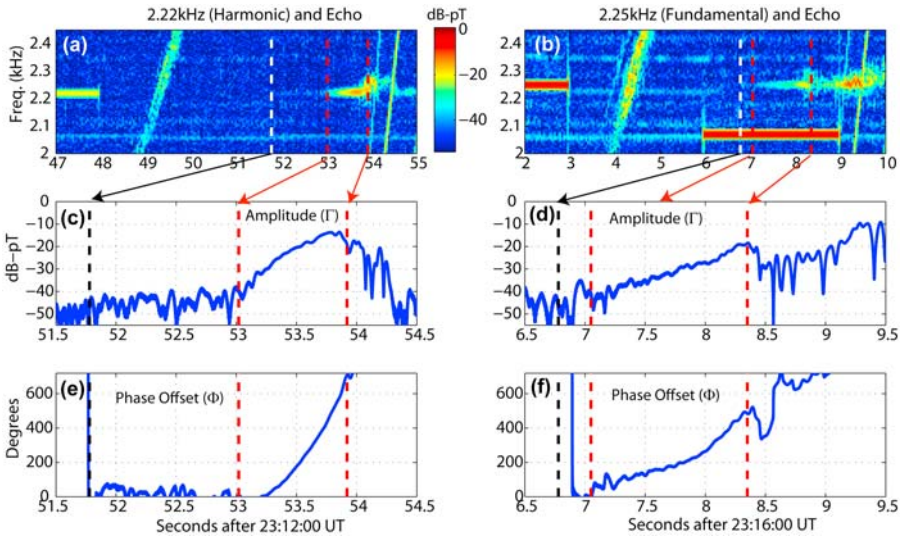


**Figure 4.** Second case of observed amplitude and phase of 2-hop echoes resulting from transmissions of a second harmonic and fundamental tone. Layout same as Figure 3.

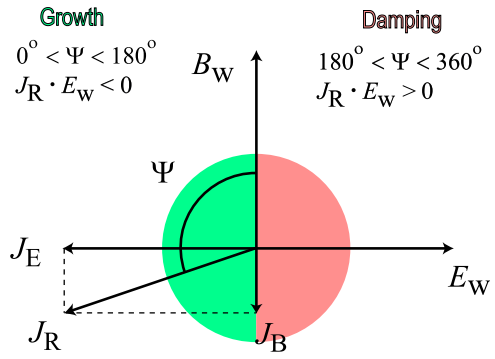


**Figure 5.** Coordinate system of vector relations between wavefields ($\mathbf{E}_w$, $\mathbf{B}_w$) and components of the nonlinear resonant current ($\mathbf{J}_R$).

linear theory in this magnetospheric channel yields a nonchanging amplitude at the ground based receiver. Furthermore, the various path losses in the experiment [*Sonwalkar et al.*, 1997] are difficult to quantify. Thus, a signal that may have experienced significant linear amplification (or damping) appears to be unchanged to the terrestrial observer. In contrast, the nonlinear interaction is distinguished by a feedback process in which the properties of the magnetospheric amplification channel change during the transmission (of a single pulse or frequency-time ramp). On the ground, the changing amplification structure manifests itself as variations in the amplitude and phase of the output signal. Observing the amplitude and phase of amplified monochromatic input signals allows for monitoring of the net changes in the interaction region.

[11] Gaining a full understanding of the space-time evolution of the amplification process requires a computer simulation, and ground based observations can be used to determine the validity of the simulation results. However, the range of outputs from these simulations can vary widely based on the initial state of the simulated plasma. The best source of plasma conditions for these simulations comes from a handful of in situ measurements of the energetic electron distribution simultaneous with observations of magnetospheric amplification [*Kimura et al.*, 1983]. However, the number of these observations near the magnetic equator in the L range of interest is very small when compared to the volume of ground based data and the variety of phenomena observed from ground based receivers. Thus, it is desirable to develop a method of estimating some parameters of the plasma involved in the interaction based on the ground observations. Understanding that the ground observations represent a "black box" view of the magnetospheric interactions, our conclusions are limited to the average or net state of the interacting plasma.

[12] Magnetospheric amplification of ELF/VLF waves is driven by counter streaming gyroresonant electrons. We analyze the observations in the context of the nonlinear theory of electron trapping in the wave potential well. The equations describing the evolution of the amplitude and phase of a narrowband ducted signal in the presence of a current constituted by resonant electrons were derived by *Nunn* [1974] and have also been employed by numerous authors [*Gibby et al.*, 2008; *Omura et al.*, 2008; *Omura and Matsumoto*, 1982; *Trakhtengerts et al.*, 2003] (see also review by *Omura et al.* [1991] and references therein). The phase $\phi$ and amplitude of the wave magnetic field $B_w$ are given by

$$\frac{dB_w}{dt} = \frac{\partial B_w}{\partial t} + v_g \frac{\partial B_w}{\partial z} = -\frac{\mu_0}{2} v_g J_E \tag{1}$$

$$\frac{d\phi}{dt} = \frac{\partial \phi}{\partial t} + v_g \frac{\partial \phi}{\partial z} = -\frac{\mu_0}{2} v_g \frac{J_B}{B_w} \tag{2}$$

where $\mu_0$ is the permeability of free space, $v_g$ is the wave group velocity and $z$ is the spatial variable along the geomagnetic field and also the wave propagation direction. The quantities $J_E$ and $J_B$ are the components of the resonant current $\mathbf{J}_R$ parallel to the wave electric $\mathbf{E}_w$ and magnetic field $\mathbf{B}_w$, respectively. Figure 5 shows the coordinate system of the vector relations. The orientation of the resonant current vector with respect to the wavefields determines whether the wave is amplified or attenuated and also the degree of phase advance. The change in wave amplitude in equation (1) can also be manipulated to express an exponential temporal growth rate $\gamma$ as shown in equation (22) of *Omura and Matsumoto* [1982] and reproduced below:

$$\gamma = \frac{1}{B_w}\frac{dB_w}{dt} = -\frac{\mu_0 v_g J_E}{2B_w} \tag{3}$$

Frequency is the rate of change of phase ($\omega = \frac{\partial \phi}{\partial t}$). Hence for linear amplification (or damping) involving no frequency change, $\frac{J_B}{B_w}$ must be constant [*Omura and Matsumoto*, 1982] necessitating that the $J_B$ component of the resonant current is initially negligible.

### 3.1. Evolution of Amplitude and Phase

[13] Ground-based observations of amplification result from dynamics that occur across a large magnetospheric interaction region that is assumed to be located near the magnetospheric equator. If the complex value $B_w^{in}$ represents the amplitude and phase of the unamplified input wave, then at the output the interaction region, the wave amplitude and phase can be expressed as

$$B_w^{out}(t) = B_w^{in} \quad \exp[\Gamma(t) + i\Phi(t)] \tag{4}$$

where $\Gamma$ is the net amplification and $\Phi$ is the phase offset from the input wave. The net amplification $\Gamma$ and phase offset $\Phi$ from the input signal as observed on the ground thus represent integrals taken along the wave propagation path

$$\Gamma = \int_0^{T_i} \gamma dt = \int_0^{T_i} -\frac{\mu_0 v_g J_E}{2B_w} dt \tag{5}$$

$$\Phi = \int_0^{T_i} \frac{d\phi}{dt} dt = \int_0^{T_i} -\frac{\mu_0 v_g J_B}{2B_w} dt \tag{6}$$

where $T_i$ is the duration of the interaction and taken to be the time it takes the wave packet to traverse the interaction region. To facilitate the discussion we represent the resonant currents by average values experienced by the wave as it propagates across the interaction region. This representation

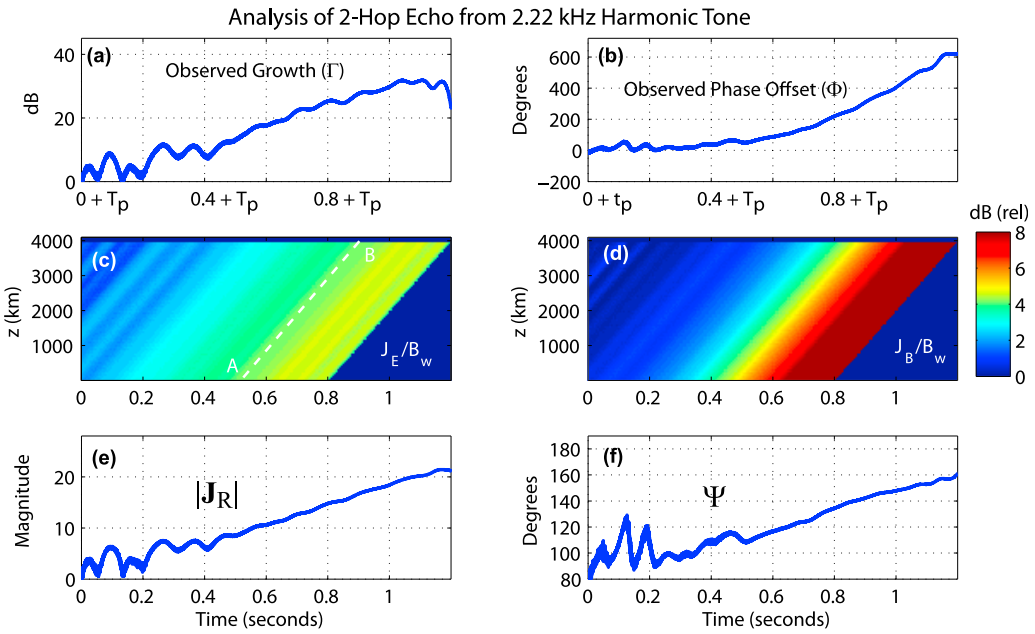


**Figure 6.** Inferred nonlinear current distribution from observed amplitude and phase of 2-hop echo induced by the second harmonic pulse shown in Figure 3 (left). (a and b) Observed growth and phase advance, respectively. (c and d) Magnetospheric current distribution if we assume uniform currents across a 4000 km long field aligned interaction region. (e and f) Inferred evolution of resonant current magnitude and phase using equations (9) and (10).

underlines the fact that ground observations give access to cumulative effects experienced by the wave. Equations (5) and (6) become

$$\Gamma = -\mu_0 v_g \left\langle \frac{J_E}{B_w} \right\rangle T_i \tag{7}$$

$$\Phi = -\mu_0 v_g \left\langle \frac{J_B}{B_w} \right\rangle T_i \tag{8}$$

where the integrals have been reduced to average values of the resonant currents over the interaction region. Although any realistic current distribution will likely exhibit a high degree of spatial and temporal variation as has been shown by computer simulations [*Gibby et al.*, 2008; *Omura and Matsumoto*, 1982], here we seek to examine the dynamics of the cumulative effects of the nonlinear current vector components that are related to the ground observations. The observed phase and amplitude can thus be used to estimate the average magnitude $\langle |\mathbf{J}_R| \rangle$ and orientation $\langle \Psi \rangle$ of the nonlinear resonant current vector as illustrated in Figure 5:

$$\langle |\mathbf{J}_R| \rangle \equiv \left\langle \sqrt{J_E^2 + J_B^2} \right\rangle \propto \sqrt{\Gamma^2 + \Phi^2} \tag{9}$$

$$\tan \langle \Psi \rangle \equiv \left\langle \frac{-J_E}{J_B} \right\rangle \simeq \frac{-\Gamma}{\Phi} \tag{10}$$

We note that the right hand side of equations (9) and (10) are approximations and not strict equivalencies since the wave amplitude ($B_w$) cannot be factored out from the integrals in (5) and (6) nor the averages in (7) and (8).

[14] Equations (9) and (10) provide for relating ground based measurements to the behavior of resonant currents in the magnetosphere. In what follows, we have chosen to discuss our observations in the context of a single equatorial crossing even though the observed 2-hop echoes have made two traversals of the equatorial plane. We assume that the wave is amplified only during the first crossing when it enters the interaction region as a coherent monochromatic pulse. The implied lack of amplification on the second crossing is supported by the strict coherence requirements of the nonlinear interaction [*Serra*, 1984; *Helliwell et al.*, 1986; *Helliwell*, 1988]. Figure 6 shows the resonant current components derived from the observation of the 2-hop echo induced by the harmonic pulse shown in Figure 3 (left). Figures 6a and 6b show the observed growth and phase offset for the interval delimited by the red dotted lines in Figures 3c and 3e, respectively. Since the wave group velocity can be calculated from the cold plasma parameters obtained in section 2, the average resonant vector components can be plotted in space and time. Figures 6c and 6d show the resonant vector components for an assumed 4000 km long interaction region beginning at the equator. The equator is the assumed starting point since most numerical simulations suggest resonant current formation to commence at or near this location [*Gibby et al.*, 2008; *Omura et al.*, 2008, 1991]. Satellite observations of chorus emissions also point to an equatorial source [*Santolík et al.*, 2003]. The main purpose of Figures 6c and 6d is to emphasize the basic geometry of the interaction in space and time.

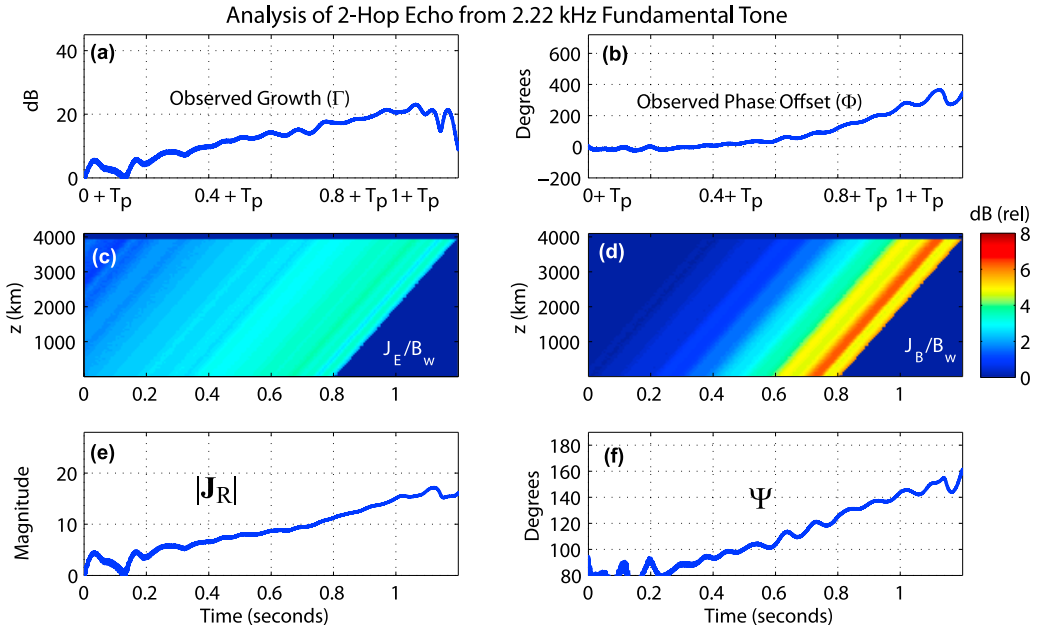


**Figure 7.** Same as Figure 6 except for the 2-hop echo resulting from the fundamental tone in Figure 3 (right).

[15] Observations on the ground are the result of integration along lines parallel to $\overline{AB}$, which corresponds to the propagation of a wave packet at the group velocity. The 4000 km extent of the interaction region is arbitrary and as mentioned above, the resonant current components are represented by average values. Figures 6e and 6f show the calculated average phase and magnitude of the nonlinear current vector as derived from the observed 2-hop echo phase and amplitude using equations (9) and (10). The time axes in Figure 6 correspond to the start of the nonlinear interaction, assumed to commence at the equator. The ground observations are made at the end of the geomagnetic field line and $T_p$ represents the propagation time from the end of the interaction region to the ground based receiver. Figure 7 shows the results for the 2-hop echo induced by the fundamental tone in Figure 3 (right) in the same format as Figure 6. In both Figure 6 and Figure 7 it can be seen that as the 2-hop echo amplitude increases, the magnitude of the resonant current vector also increases and the phase angle ($\Psi$) approaches 180°. This occurs because the phase offset of the observed echoes, which is driven by $J_B$, outpaces the amplitude growth, which is driven by $J_E$, yielding a rotation of the nonlinear resonant current vector. This rotation of the nonlinear current vector is consistent with the theoretical expectations since after its growth phase the 2-hop echo amplitude is seen to saturate and attenuate, manifested by the resonant current vector surpassing 180° in phase (see Figure 5). In fact, the inferred rotation of the resonant current vector has been predicted by numerical models. *Omura and Summers* [2006] report the rotation of the net resonant current vector as manifested by an "electron phase space hole." Likewise, *Gibby et al.* [2008] directly attribute rotation of the resonant current vector to the mechanism of amplitude saturation. The concept of rotation of the nonlinear current vector leading to amplitude saturation can readily be seen in the coordinate system in Figure 5. If the resonant current vector (created by an electron phase space hole) is between 180° and 360° then the wave-particle interaction yields damping and not growth. It is the damping action of the nonlinear currents that *Gibby et al.* [2008] attribute to amplitude saturation.

### 3.2. Estimation of Linear Growth Rate

[16] We next turn our attention to the additional delay of the 2-hop echo resulting from the lower input amplitude of the harmonic pulse. We note that for both input amplitudes (fundamental and harmonic tones) the onset of 2-hop echo observation on the ground corresponds to commencement of nonlinear growth since the rate of phase advance for both cases (Figures 6b and 7b) is 1–2 Hz and likewise the amplitude in both cases (Figures 6a and 7a) is below saturation. *Paschal and Helliwell* [1984] document how the initial phase advance for ground observations of nonlinear growth is on the order of 1–3 Hz during the first 500 ms followed by acceleration of phase advance to 60–120 Hz. If the 2-hop echo observed from the lower input amplitude were simply observed later because it started growing from a lower initial level (below the noise floor) then its frequency at the onset of observation would be removed by tens of Hz from the input frequency, which it is not. The delay in the 2-hop echo is thus apparently connected to the onset of nonlinear growth. The existence of an amplitude threshold for nonlinear growth has been shown theoretically [*Omura et al.*, 1991, and references therein] and also experimentally [*Helliwell et al.*, 1980]. The amplitude threshold or "trapping amplitude" for nonlinear growth corresponds to the minimum amplitude needed to overcome the geomagnetic inhomogeneity and "phase trap" energetic electrons in the magnetic potential well of the wave. *Nunn* [1974] postulates that triggering delay can result from input amplitudes initially below the trapping amplitude and therefore needing amplitude growth in the linear regime

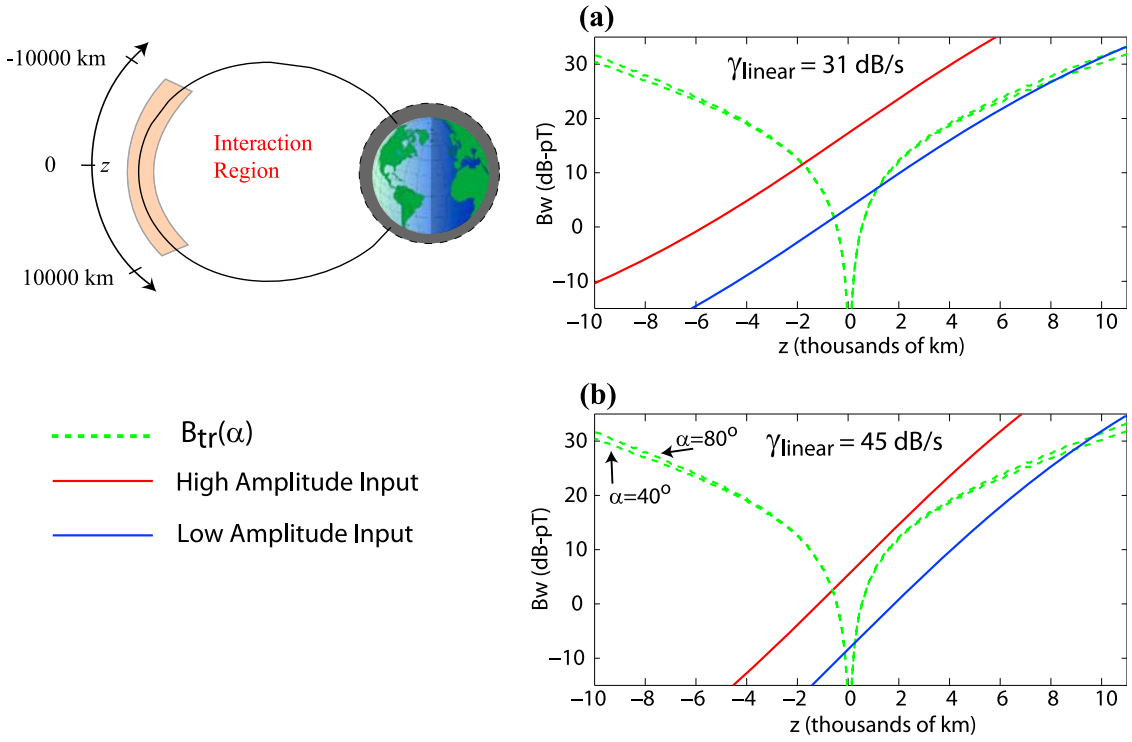


**Figure 8.** Schematic of interaction region and two boundary estimates of initial input amplitudes and linear growth rates such that the higher amplitude input exceeds the trapping threshold ($B_{tr}$) everywhere past the equator and the lower input amplitude only close to 10,000 km (excluding the singularity at the equator). The parameter $\alpha$ is the electron pitch angle.

before the nonlinear threshold is reached. Such a hypothesis is bolstered by a numerical model sensitivity study presented by *Gibby* [2008] which shows that a lower linear growth rate or a lower input amplitude would both lead to a delayed echo observation at the output of the interaction region.

[17] Since the magnetospheric path and cold plasma parameters are accessible from the dispersion analysis discussed in section 2, it is possible to use the observed amplitude-dependent onset delay to estimate the linear magnetospheric growth rate. If the amplitude threshold for nonlinear growth were constant along the magnetospheric path then the observed 1 s onset delay for the 13.8 dB lower input would imply a 13.8 dB/s linear growth rate. However, the minimum wave amplitude for electron phase trapping by a constant frequency wave is a strong function of position along the field line and can be shown to be [*Bell and Inan*, 1981]

$$B_{tr} = \frac{-m_e}{qk\mathrm{v_R}\tan\alpha} \cdot \left\{ \left[ \frac{3}{2}\mathrm{v_R} - \frac{k(\mathrm{v_R}\tan\alpha)^2}{2\omega_c} \right] \frac{\partial\omega_c}{\partial z} - \mathrm{v_R}\frac{(\omega_c-\omega)}{\omega_p}\frac{\partial\omega_p}{\partial z} \right\} \quad (11)$$

$$\mathrm{v_R} = \frac{\omega-\omega_c}{k} \quad (12)$$

where $\omega$ and $k$ are the wave frequency and wave number, respectively, $\omega_c$ is the cyclotron frequency, $\omega_p$ is the electron plasma frequency, and $\alpha$ is the electron pitch angle. The derivation of equation (11) includes the contribution of cold plasma density gradients that are often neglected. Figure 8 shows plots of the trapping amplitude ($B_{tr}$) as a function of distance along the geomagnetic line for two local pitch angles for the $L$ shell and cold plasma density discussed in section 2. High pitch angle ($\alpha > 60°$) electrons are believed to drive wave growth [*Bell et al.*, 2000] making the 40° and 80° pitch angles in Figure 8 representative of the likely limits of this parameter. We note that there is little difference between the curves for the two pitch angles. Under these propagation conditions, the 1 s onset delay corresponds to a ~10,000 km propagation distance for a whistler wave at ~2 kHz near the geomagnetic equator. Figure 8 shows an interaction region extending 10,000 km on either side of the geomagnetic equator, with red and blue lines showing the effect of linear growth on the leading edges of the high-amplitude (2250 Hz) and low-amplitude (2220 Hz) pulses, respectively. The initial amplitudes of the pulses are set so that they are 13.8 dB apart, consistent with the observations in section 2. We further assume that the amplitude of the high-amplitude pulse exceeds the nonlinear threshold near the magnetic equator and remains above the threshold for some distance longer than the region shown. Thus, the high-amplitude pulse begins sustained nonlinear growth shortly after the leading edge of the pulse crosses the equator. Conversely, the weaker pulse does not exceed the nonlinear threshold (except briefly at the equator) until 10,000 km past the equator. Such a scenario yields two bounding estimates of the linear growth rate and wave input amplitudes at the start of the interaction region shown in Figures 3a and 3b. The wave input amplitudes are 18–300 fT

and 4–61 fT for the strong and weak pulses, respectively, and the linear growth rate is 31–45 dB/s. The scenario presented above would lead to the observed onset delay only if crossing the trapping threshold at 10,000 km would instantaneously lead to nonlinear growth at the equator that is subsequently observed on the ground. As in section 3.1 we accept that initial observed nonlinear growth with frequency close to the input frequency is generated close to the equator. Although the counterstreaming gyroresonance condition intrinsically causes resonant currents to propagate in a direction opposite to the input wave, their arrival at the equator requires a finite time. Our linear growth estimates should thus be interpreted as lower bounds since it is possible and even likely that the weaker pulse begins to exceed the trapping threshold closer to the equator.

## 4. Discussion and Summary

[18] We present new observations from the HAARP wave injection experiment involving the interpretation of the joint variation of amplitude and phase of nonlinearly amplified signals and the estimation of the linear magnetospheric growth rate. This represents the first interpretation of ground observations in the context of the evolution of nonlinear resonant currents. In our analysis we have interpreted phase advance to result from the $J_B$ component of the resonant current in accord with the majority of theoretical work on magnetospheric amplification of monochromatic input waves [*Omura et al.*, 1991; *Gibby et al.*, 2008]. As our observations show, after commencement of nonlinear growth, phase advance accelerates and subsequently leads to rapidly changing frequency risers. It is worth noting that in recent work on spontaneously radiating chorus waves (no monochromatic input), *Omura et al.* [2008] claim that the $J_B$ contribution to frequency sweep rate is negligible. The specific role of the $J_B$ component in the initial formation of radiating resonant currents may be a key difference between amplification of man-made and natural (chorus) waves that otherwise have many similar characteristics. A related point of contrast between chorus and amplified emissions of anthropogenic origin may be the propagation mode of these waves in the magnetosphere. Ground based observations of man-made signals, including those presented here, corroborate a ducted field-aligned propagation mode. Likewise, finite computing resources have necessitated that most numerical simulations also focus on the one-dimensional field-aligned problem. Even though satellite observations have illuminated 3-D aspects of chorus propagation [*Santolík and Gurnett*, 2003; *Platino et al.*, 2006], the extent to which the model of ducted propagation can be extended to chorus observations continues to be the subject of active research [*Gołkowski and Inan*, 2008; *Bell et al.*, 2009].

[19] The linear magnetospheric growth rate and the energetic electron distribution from which it derives are both fundamental unknowns that are difficult to measure yet play central roles in magnetospheric amplification processes. The analysis presented in this paper offers new approaches for assessing the energetic electron distribution from ground based measurements and is a key contribution of this paper. Quantification of the energetic plasma distribution remains a key task in calibrating models and shedding light on fundamental processes in the magnetosphere. In this context we note that *Kimura et al.* [1983] report maximum linear growth rates of 6–43 dB/s from in situ measurements and numerical studies have employed a wide range of growth rates from 60 to 350 dB/s [*Nunn et al.*, 2005; *Gibby et al.*, 2008]. Ground based observations may therefore serve to improve such estimates. In future experiments, successive tones of finely varying amplitude (1–2 dB) will be transmitted to investigate more thoroughly the associated delay of nonlinear growth initiation. Moreover, numerical simulation of the observed cases will be pursued to validate the linear growth estimates.

[20] **Acknowledgments.** This work was supported by the High Frequency Active Auroral Research Program (HAARP), the Defense Advanced Research Programs Agency (DARPA), and by the Office of Naval Research (ONR) via ONR grant N0001405C0308 to Stanford University. The authors would like to thank the HAARP operators Mike McCarrick, Helio Zwi, and David Seafolk-Kopp for realization of this experiment.

[21] Amitava Bhattacharjee thanks the reviewers for their assistance in evaluating this paper.

## References

Angerami, J. J., and J. O. Thomas (1964), Studies of planetary atmospheres, *J. Geophys. Res.*, *69*, 4537–4560.

Barr, R., and P. Stubbe (1993), ELF harmonic radiation from the Troms(ø) heating facility, *Geophys. Res. Lett.*, *20*, 2243–2246.

Bell, T. F., and U. S. Inan (1981), Transient nonlinear pitch angle scattering of energetic electrons by coherent VLF wave packets in the magnetosphere, *J. Geophys. Res.*, *86*, 9047–9063.

Bell, T. F., U. S. Inan, R. A. Helliwell, and J. D. Scudder (2000), Simultaneous triggered VLF emissions and energetic electron distributions observed on POLAR with PWI and HYDRA, *Geophys. Res. Lett.*, *27*, 165–168.

Bell, T. F., U. S. Inan, N. Haque, and J. S. Pickett (2009), Source regions of banded chorus, *Geophys. Res. Lett.*, *36*, L11101, doi:10.1029/2009GL037629.

Carpenter, D. L. (1980), Fast fluctuations in the arrival bearing of magnetospherically propagating signals from the Siple, Antarctica, VLF transmitter, *J. Geophys. Res.*, *85*, 4157–4166.

Carpenter, D. L., V. S. Sonwalkar, R. A. Helliwell, M. Walt, U. S. Inan, M. Ikeda, and D. L. Caudle (1997), Probing properties of the magnetospheric hot plasma distribution by whistler mode wave injection at multiple frequencies: Evidence of spatial as well as temporal wave growth, *J. Geophys. Res.*, *102*, 14,355–14,362.

Cohen, M. B., M. Gołkowski, and U. S. Inan (2008), Orientation of the HAARP ELF ionospheric dipole and the auroral electrojet, *Geophys. Res. Lett.*, *35*, L02806, doi:10.1029/2007GL032424.

Cohen, M. B., U. S. Inan, and E. Paschal (2009), Sensitive broadband ELF/VLF radio reception with the AWESOME instrument, *IEEE Trans. Geosci. Remote Sens.*, *48*, 3–17, doi:10.1109/TGRS.2009.2028334.

Dowden, R. L., A. D. McKay, L. E. S. Amon, H. C. Koons, and M. H. Dazey (1978), Linear and nonlinear amplification in the magnetosphere during a 6.6-kHz transmission, *J. Geophys. Res.*, *83*, 169–181.

Gibby, A. R. (2008), Saturation effects in VLF triggered emissions, Ph.D. thesis, Stanford University, Stanford, Calif.

Gibby, A. R., U. S. Inan, and T. F. Bell (2008), Saturation effects in the VLF-triggered emission process, *J. Geophys. Res.*, *113*, A11215, doi:10.1029/2008JA013233.

Gołkowski, M., and U. S. Inan (2008), Multistation observations of ELF/VLF whistler mode chorus, *J. Geophys. Res.*, *113*, A08210, doi:10.1029/2007JA012977.

Gołkowski, M., U. S. Inan, A. R. Gibby, and M. B. Cohen (2008), Magnetospheric amplification and emission triggering by ELF/VLF waves injected by the 3.6 MW HAARP ionospheric heater, *J. Geophys. Res.*, *113*, A10201, doi:10.1029/2008JA013157.

Hayakawa, M., and S. S. Sazhin (1992), Mid-latitude and plasmaspheric hiss: A review, *Planet. Space Sci.*, *40*, 1325–1338.

Helliwell, R. A. (1988), VLF wave simulation experiments in the magnetosphere from Siple Station, Antarctica, *Rev. Geophys.*, *26*(3), 551–578.

Helliwell, R. A., and J. P. Katsufrakis (1974), VLF wave injection into the magnetosphere from Siple Station, Antarctica, *J. Geophys. Res.*, *79*, 2511–2518.

Helliwell, R. A., D. L. Carpenter, and T. R. Miller (1980), Power threshold for growth of coherent VLF signals in the magnetosphere, *J. Geophys. Res.*, *85*, 3360–3366.

Helliwell, R. A., U. S. Inan, J. P. Katsufrakis, and D. L. Carpenter (1986), Beat excitation of whistler mode sidebands using the Siple VLF transmitter, *J. Geophys. Res.*, *91*, 143–153.

Hobara, Y., V. Y. Trakhtengerts, A. G. Demekhov, and M. Hayakawa (2000), Formation of electron beams under the interaction of a whistler wave packet with the radiation belt electrons, *J. Atmos. Solar-Terr. Phys.*, *62*, 541–552.

Inan, U. S., T. F. Bell, J. Bortnik, and J. M. Albert (2003), Controlled precipitation of radiation belt electrons, *J. Geophys. Res.*, *108*(A5), 1186, doi:10.1029/2002JA009580.

Karpman, V. I., J. N. Isotomin, and D. R. Shklyar (1975), Effects of nonlinear interaction of monochromatic waves with resonant particles in the inhomogeneous plasma, *Phys. Scr.*, *11*, 278–284.

Kennel, C. F., and H. E. Petschek (1966), Limit on stably trapped particle fluxes, *J. Geophys. Res.*, *71*, 1–28.

Kimura, I., H. Matsumoto, T. Mukai, K. Hashimoto, T. F. Bell, U. S. Inan, R. A. Helliwell, and J. P. Katsufrakis (1983), EXOS-B/Siple Station VLF wave-particle interaction experiments: 1. General description and wave-particle correlations, *J. Geophys. Res.*, *88*, 282–294.

Nunn, D. (1974), A self-consistent theory of triggered VLF emissions, *Planet. Space Sci.*, *22*, 349–378.

Nunn, D., M. Ryroft, and V. Trakhtengerts (2005), A parametric study of the numerical simulations of triggered VLF emissions, *Ann. Geophys.*, *23*, 1–12.

Omura, Y., and H. Matsumoto (1982), Computer simulations of basic processes of coherent whistler wave-particle interactions in the magnetosphere, *J. Geophys. Res.*, *87*, 4435–4444.

Omura, Y., and D. Summers (2006), Dynamics of high-energy electrons interacting with whistler mode chorus emissions in the magnetosphere, *J. Geophys. Res.*, *111*, A09222, doi:10.1029/2006JA011600.

Omura, Y., H. Matsumoto, D. Nunn, and M. J. Rycroft (1991), A review of observational, theoretical and numerical studies of VLF triggered emissions, *J. Atmos. Terr. Phys.*, *53*, 351–368.

Omura, Y., N. Furuya, and D. Summers (2007), Relativistic turning acceleration of resonant electrons by coherent whistler mode waves in a dipole magnetic field, *J. Geophys. Res.*, *112*, A06236, doi:10.1029/2006JA012243.

Omura, Y., Y. Katoh, and D. Summers (2008), Theory and simulation of the generation of whistler-mode chorus, *J. Geophys. Res.*, *113*, A04223, doi:10.1029/2007JA012622.

Paschal, E. W., and R. A. Helliwell (1984), Phase measurements of whistler mode signals from the Siple VLF transmitter, *J. Geophys. Res.*, *89*, 1667–1674.

Piddyachiy, D., U. S. Inan, T. F. Bell, N. G. Lehtinen, and M. Parrot (2008), DEMETER observations of an intense upgoing column of ELF/VLF radiation excited by the HAARP HF heater, *J. Geophys. Res.*, *113*, A10308, doi:10.1029/2008JA013208.

Platino, M., U. S. Inan, T. F. Bell, J. S. Pickett, and P. Canu (2006), Rapidly moving sources of upper band ELF/VLF chorus near the magnetic equator, *J. Geophys. Res.*, *111*, A09218, doi:10.1029/2005JA011468.

Raghuram, R., R. L. Smith, and T. F. Bell (1974), VLF antarctic antenna: Impedance and efficience, *IEEE Trans. Antennas Propag.*, *22*, 334–338.

Santolík, O., and D. A. Gurnett (2003), Transverse dimensions of chorus in the source region, *Geophys. Res. Lett.*, *30*(2), 1031, doi:10.1029/2002GL016178.

Santolík, O., D. A. Gurnett, J. S. Pickett, M. Parrot, and N. Cornilleau-Wehrlin (2003), Spatio-temporal structure of storm-time chorus, *J. Geophys. Res.*, *108*(A7), 1278, doi:10.1029/2002JA009791.

Sazhin, S. S., and M. Hayakawa (1992), Magnetospheric chorus emissions: A review, *Planet. Space Sci.*, *40*, 681–697.

Sazhin, S. S., M. Hayakawa, and K. Bullough (1992), Whistler diagnostics of magnetospheric parameters: A review, *Ann. Geophys.*, *10*, 293–308.

Serra, F. M. (1984), VLF two-wave-electron interactions in the magnetosphere, *Planet. Space Sci.*, *32*, 985–1005.

Sonwalkar, V. S., D. L. Carpenter, R. A. Helliwell, M. Walt, U. S. Inan, D. L. Caudle, and M. Ikeda (1997), Properties of the magnetospheric hot plasma distribution deduced from whistler mode wave injection at 2400 Hz: Ground-based detection of azimuthal structure in magnetospheric hot plasmas, *J. Geophys. Res.*, *102*, 14,363–14,380.

Stiles, G. S., and R. A. Helliwell (1975), Frequency-time behavior of artificially stimulated VLF emissions, *J. Geophys. Res.*, *80*, 608–618.

Storey, L. R. O. (1953), An investigation of whistling atmospherics, *Philos. Trans. R. Soc. London, Ser. A*, *246*, 113–141.

Trakhtengerts, V. Y., A. G. Demekhov, Y. Hobara, and M. Hayakawa (2003), Phase-bunching effects in triggered VLF emissions: Antenna effect, *J. Geophys. Res.*, *108*(A4), 1160, doi:10.1029/2002JA009415.

M. B. Cohen, M. Gołkowski, and U. S. Inan, STAR Laboratory, Stanford University, Stanford, CA 94305, USA. (golkowski@gmail.com)

A. R. Gibby, Arion Systems Inc., 15040 Conference Center Dr., Ste. 200, Chantilly, VA 20151, USA.